

A CFD STUDY OF THE ACTIVE FLOW CONTROL SYSTEM BEHAVIOUR ON A VERTICAL TAIL SECTION OF AN AIRPLANE, WITH THE AID OF AI

Carlo Cordoni¹, Antonio Saporiti¹ & Maurizio Boffadossi¹

¹ DAER, Politecnico di Milano, Via La Masa 34, 20156 Milano, Italy

Abstract

A Machine Learning (ML) methodology was exploited to predict the aerodynamic performances of a 2D vertical tail section (VTS) of an airplane with an Active Flow control (AFC) device installed near the hinge of the rudder. In the 2D section, this AFC device, similar to a Sweeping Jet, is modelled by a set of local boundary conditions applied to the URANS solver. In particular, the ejected velocities are modelled as square wave function of time for different frequencies f (50,100,150 Hz), at several maximum values v_{MAX} (0, 10, 25, 50, 75, 100 m/s). Computational Fluid Dynamics (CFD) runs have been accomplished for sideslip angles β of 0°, 5°, 10° and rudder deflections δ of 0°, 10° and 20°, for each square wave profile of the SJ velocity, at Reynolds' number (Re) 15 million and Mach number (M) 0.15. The aerodynamic coefficients (CI, Cd, Cm) gathered by the CFD were then exploited to train a feed-forward Neural Network (NN) of 4 inputs (β , δ , ν_{MAX} , f), one level of 10 neurons, and 3 outputs (Cl, Cd, Cm). The network was then able to correctly match the CFD prediction values. Moreover, the trained NN was employed for retrieving intermediate flow conditions not covered by the previous CFD analysis with the aim to get either a sideforce enhancement of 20%, for selected sideslip and rudder deflection angles, or a target lift coefficient of 1.5 at minimum drag. The advantages of this machine learning methodology were twofold: to obtain the aerodynamic coefficients within the entire flight envelope of an airplane (i.e. Pressure Altitude vs. Outside Ambient Temperature, Mach vs Reynolds Number) once the boundary and some few inner points have been calculated by CFD, to predict the optima SJ parameters as needed for the Lift enhancement in the flight spectrum. The negligible CPU time, with respect to a pure-CFD approach is an added value of this approach.

Keywords: Artificial Intelligence, Machine-Learning, Neural-Network, Active-Flow-Control, Sweeping-Jet, Fluidic-Oscillator, Computational-Fluid-Dynamics, Tail-Vertical-Surface

Nomenclature

CFD = Computational Fluid Dynamics

AI = Artificial Intelligence

ML = Machine Learing

SJ = Sweeping Jet

AFC = Active Flow Control

NN = Neural Network

OEI = One Engine Inoperative

URANS = Unsteady Reynolds Averaged Navier-Stokes

MSE = Mean Square Error

f = sweeping frequency [Hz]

 v_{MAX} = maximum ejection velocity [m/sec]

 β = sideslip angle [deg]

 δ = rudder deflection [deg]

CI = lift coefficient

Cd = drag coefficient

Cm = moment coefficient

 ΔC_v = sideforce enhancement

 α = angle of attack [deg]

Re = Reynolds number

M = Mach number

OAT = Outside Air Temperature [K]

SST = Shear Stress Transport

k = Turbulent Kinetic Energy [m²/sec²]

 ω = Specific Turbulent Dissipation Rate [1/sec]

%t = time of ejection over the ejection period, in percentage

P =power of the ejected jet

 C_{π} = power coefficient of P

E = energy of the ejected jet over one period

 C_E = energy coefficient of E

1. Introduction

The vertical tail surface of an airplane is commonly designed in order to guarantee controllability and operability even when emergency conditions (i.e. One Engine Inoperative, OEI, at the take-off, Figure 1.1) occur, so that safety certification or qualification rules are satisfied. Consequently, the tail unit has to 'passively' counteract any possible induced flight drawbacks to guarantee the required aerodynamic performance to sustain the flight or the recovery manoeuvres. This drives the geometric size of the vertical tail unit, with associated large surfaces that impacts on weight and drag, translating in higher fuel consumption. One possible way to overcome this issue, thereby having a smaller surface, is the application of Sweeping Jets (SJ) devices [1], that allow to manage the effectiveness of the vertical tail surface by guarantying the necessary side force by means of delaying separation. These devices have an internal shape that creates a periodic plane sweeping jet as an output, Figure 1.2. Although they do need a compressed steady supply of air at high pressure, the advantages are their applicability to high Reynolds number regimes and the lower mass flow rates with respect to continuous blowing devices [2]; in addition, these objects are robust, as they have no moving parts, being the sweeping effect created by the internal geometry itself.

Sweeping jets were successfully tested on full-scale wind tunnel tail model of a Boeing 757 airplane [3] and their effectiveness was proved by the Boeing 757 eco-Demonstrator flight in 2015 [4].

Extensive studies have been performed in the last decade to assess the flow behaviours and performance of those devices [8], [9], [10], [11], [13], [14], [15], [16], [18], [19], [20], [21], while an interesting review of both passive and active flow control technique can be find in [12].

In this work, the application of the Active Flow Control to the vertical tail of an airplane was modelled by a simplified 2D methodology: in particular, the final goal was to investigate a procedure for exploiting Machine Learning (ML) to predict the aerodynamic performances of a modified NACA 0012 airfoil with a AFC device applied at the hinge of the rudder. The mean aerodynamic chord ($c_{MAC} = 4.5 \, m$) was been set as that of the Boeing 757. The sweeping jet modulus of the velocity of ejection was modelled, on the 2D section, by a square wave as a function of time, and its direction was parallel to the chord of the airfoil: the exhaust flow was imposed as a boundary condition perpendicular to a step of 0.9 cm at the hinge of the rudder (see the line in bold red in Figure 1.3). The frequency f of this wave was studied in a range between 50 Hz and 150 Hz and its maximum velocity v_{MAX} between 0 m/s and 100 m/s.

CFD simulations were run with ANSYS FLUENT© for three sideslip angles β (0°, 5°, 10°) and for three rudder deflections δ (0°,10°, 20°), at different actuation regimes (v_{MAX} , f). CFD aerodynamic coefficients were collected in a dataset to feed a machine learning MATLAB© tool for training a Neural Network (NN).

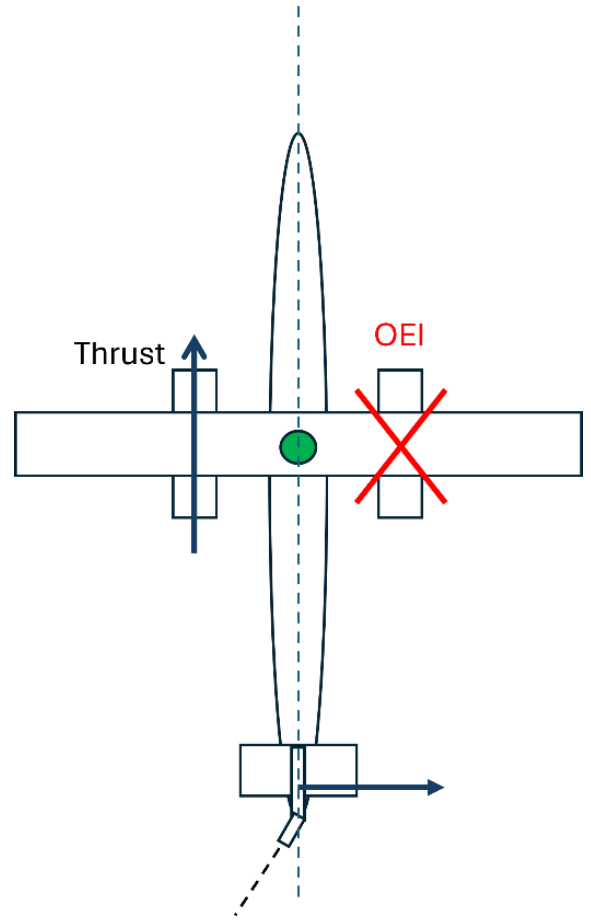


Figure 1.1 - Balance around the yaw axes, OEI condition at the take-off

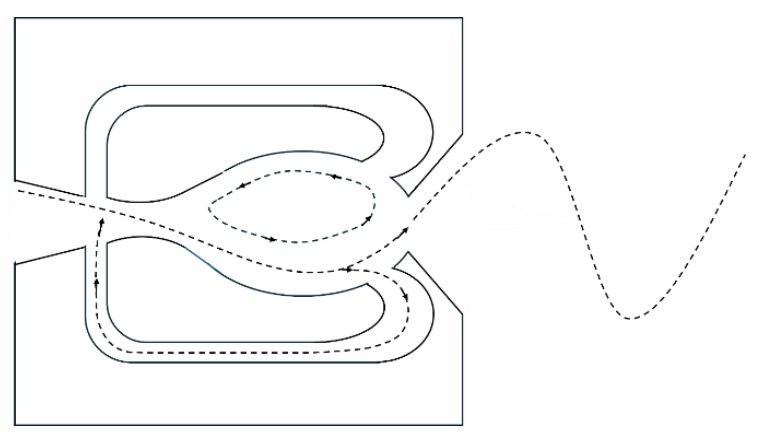


Figure 1.2 - Sweeping jet scheme, top view

Once the NN was validated by matching the CFD database, the NN was then successfully used to predict, at the same Re and Mach of the CFD database, the aerodynamic performances (frequency and exit velocity) of the SJ for two aims: firstly, to increment the lift coefficient of the tail section of 20%, for sideslip angles β from 0° to 10°, and for rudder deflections δ from 10° to 20°; secondly, to obtain as a target Cl=1.5 with the lowest drag. This paper is based on a Master thesis [22] of the corresponding author (section 6).

The structure of the paper is as follows: in section 2 the base theory of the Neural Network is reviewed, a summary on the numerical procedures is shown in section 3, the main results are reported in section 4, conclusions and follow-on are presented in section 5.

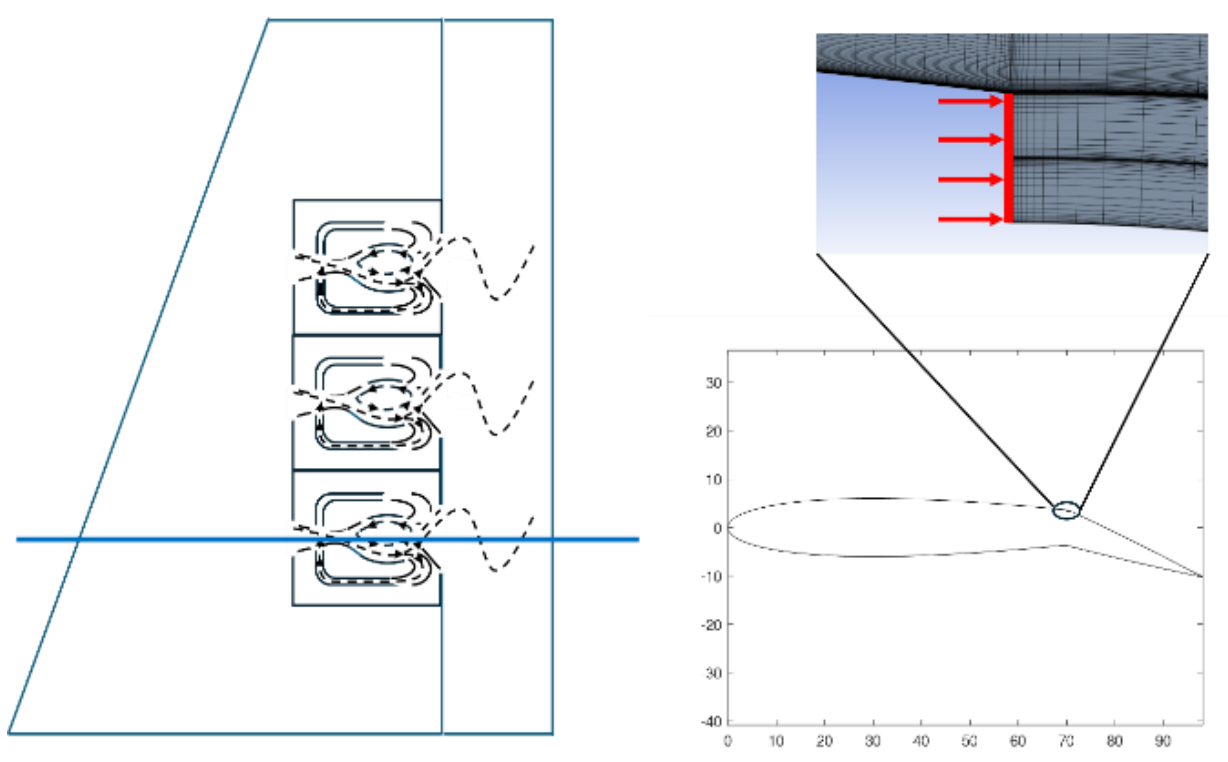


Figure 1.3 - 2D simplified modeling of the SJ action in a plane perpendicular to the vertical tail surface

2. Neural Network

A feed-forward neural network (NN) is a simplified imitation of what happens in the brain: inputs x_i are connected to a layer of neurons, Figure 2.1, and each subsequent layer has a connection from the previous layer, until the layer of the outputs.

The NN of this paper has one layer of 10 neurons, 4 inputs (β , δ , v_{MAX} ,f), and 3 outputs, (Cl, Cd, Cm). Each neuron sums up the inputs and it generates a signal F_j through a sigmoid activation function, (1). Finally, the outputs to the net are obtained as a linear combination of F_i ,(2).

$$F_i(x_1, \dots) = \sigma(\sum_i w_{ii} x_i + b_i)$$
(1)

$$o_z = \sum_j w_{zj} F_j + b_z \tag{2}$$

2.1 Training algorithm

It is defined a quantity V(x), (3), as the sum of the errors between the predicted outputs by the net and the target outputs of the dataset. It follows $\nabla V(x) = \mathbf{J}^{\mathsf{T}}(x) e(x)$, being **J** the Jacobian of the errors e(x) with respect to some vector x.

$$V(\mathbf{x}) = \sum_{l} e_{l}^{2} (\mathbf{x}) \tag{3}$$

The training of the neural network is based on the Levenberg-Marquardt algorithm [5], (4).

$$x_{t+1} = x_t - \left(\mathbf{J}^{\mathsf{T}}\mathbf{J} + \tau\mathbf{I}\right)^{-1}\mathbf{J}^{\mathsf{T}}e \tag{4}$$

Where x_t is the vector of weights and offsets of the net at the time step t, and τ is a parameter.

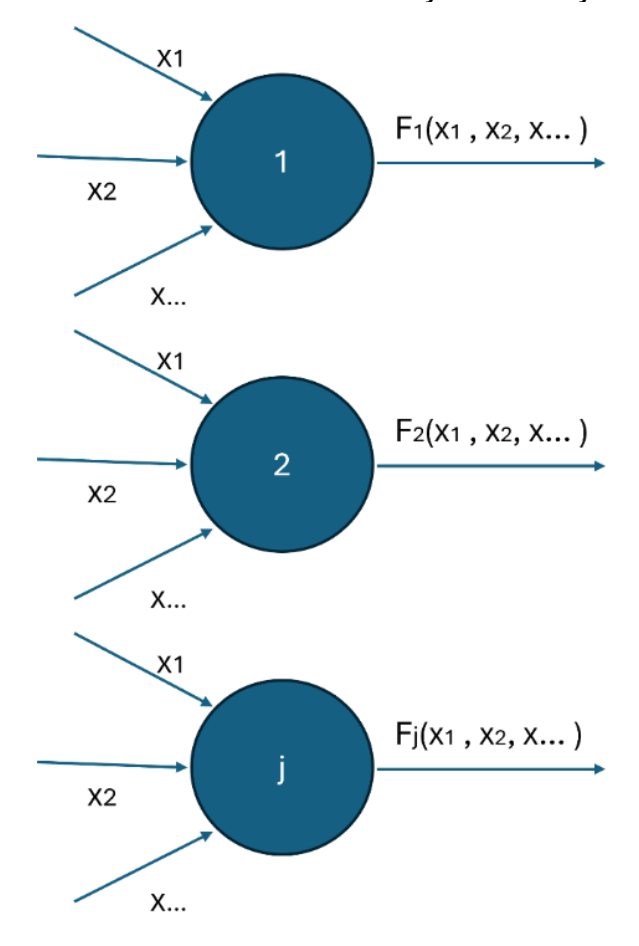


Figure 2.1 - layer of neurons

The value of τ is updated each iteration: if V(x) increases, τ increases as well; if V(x) decreases, τ is reduced. V(x), (3), is a measure of the goodness of the network: the lower it becomes, the lower the associate error between predictions and target outputs. The back-propagation algorithm [5] is used to compute the matrix \mathbf{J} .

It is useful to define a performance index of the network as the mean squared error (MSE), (5).

$$MSE = \frac{1}{2N}V(x) \tag{5}$$

Where N is the total number of outputs of the training dataset.

The training stops when the MSE does not decrease anymore.

3. CFD settings

Within the ANSYS FLUENT © environment, the chosen numerical method for this study was based on U-RANS equations. The fluid is an ideal gas which follows the Sutherland's law for viscosity. The turbulence is modelled with the K- ω SST model [17]. The formulation is pressure based and the energy equation is on. The second order Roe upwind scheme is used in space. The time stepping is second order implicit. Boundary conditions of the entire domain are reported in Table 1, and the Active Flow Control (AFC) Device velocity profile was imposed at the step close to the hinge, Figure 3.1.

The red velocity profile of Figure 3.1 is a square wave function of time, Figure 3.2: on the x axes, the time is in seconds; on the y axes, the jet velocity is dimensionless with respect to the v_{MAX} of the current simulation.

The chosen flight condition for analysis is a take-off at sea level, OAT=300 K, M=0.15, Re (Fin chord based) =15million.

_			
T_{α}	h	\sim	1
1 1			- 1

1 45.0				
Domain INLET	1 atm, 300 K, M = 0.15, β			
Domain OUTLET	1 atm, 300 K, M = 0.15, β			
AIRFOIL	Adiabatic, no slip			
Flow-Control-Device	Velocity profile perpendicular to the step, 300K			

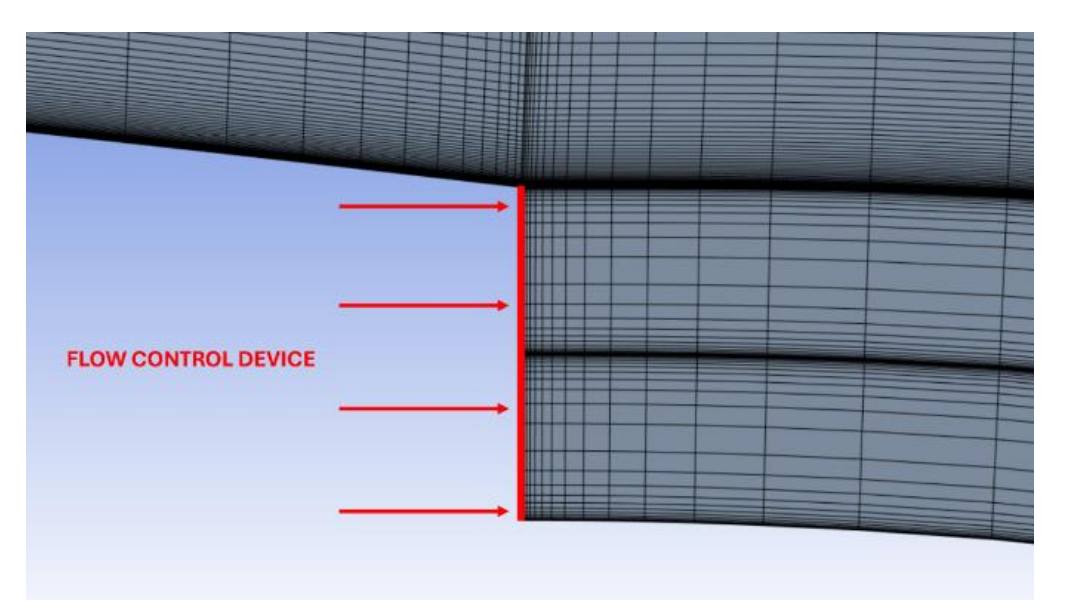


Figure 3.1 - Fluidic Actuator, Velocity Boundary condition

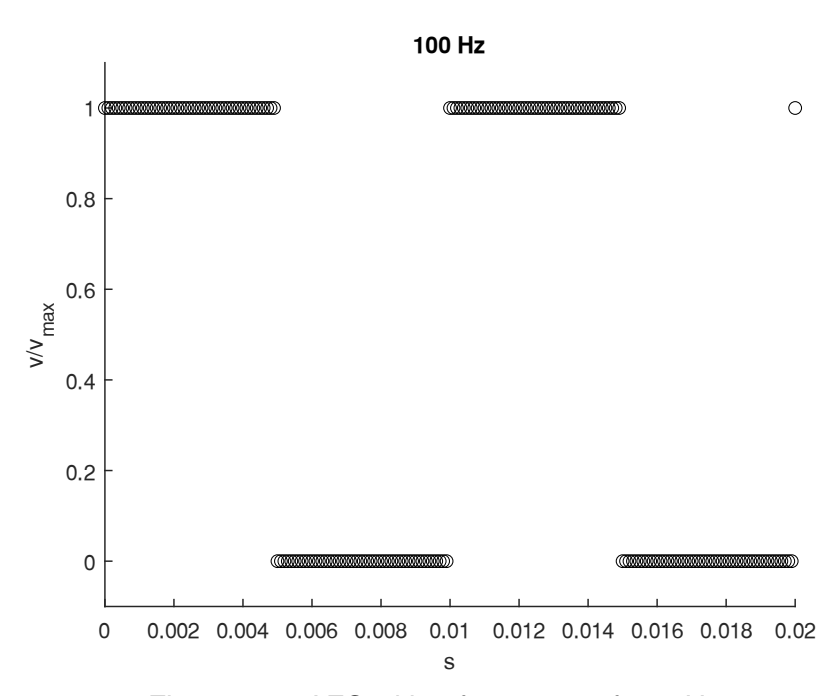


Figure 3.2 - AFC with a frequency of 100 Hz

The numerical procedures were validated both against experimental data [6] and through grid convergence procedures.

In Table 2, lift and drag coefficients from CFD are compared to data from experiments [6], where the angle of attack is α (deg). Lift results are about 1% error; drag coefficient is well computed as well. CFD results capture both the correct slope of the curve, when linear behaviour happens, and the stall condition at about angle of attack α =16°, Figure 3.3, where the different maximum value of lift coefficient is the same of experimental uncertainties, as mentioned in [7]. In Figure 4.1, the Cd-Cl

curve shows that the Cd behaviour is matched as well.

Table 2							
α	CI	Cd	Ladson Cl	Ladson Cd			
0°	-6.730e-7	0.802e-2	1.150e-2	0.803e-2			
10°	1.092	1.248e-2	1.080	1.165e-2			
15°	1.523	2.335e-2	1.517	1.870e-2			

To train the NN, the total number of data points which were simulated for Re= 15 million and M= 0.15 is 162, as follows:

- 3 angles of sideslip β 0°,5°,10°,
- 3 angles of deflection δ 0°,10°,20°
- 6 values of the v_{MAX} of the AFC system 0 m/s, 10 m/s, 25 m/s, 50 m/s, 75 m/s, 100 m/s
- 3 values of the frequency of the AFC system 50 Hz, 100 Hz, 150 Hz

CFD aerodynamic coefficients were used to build the dataset for the training of the neural network.

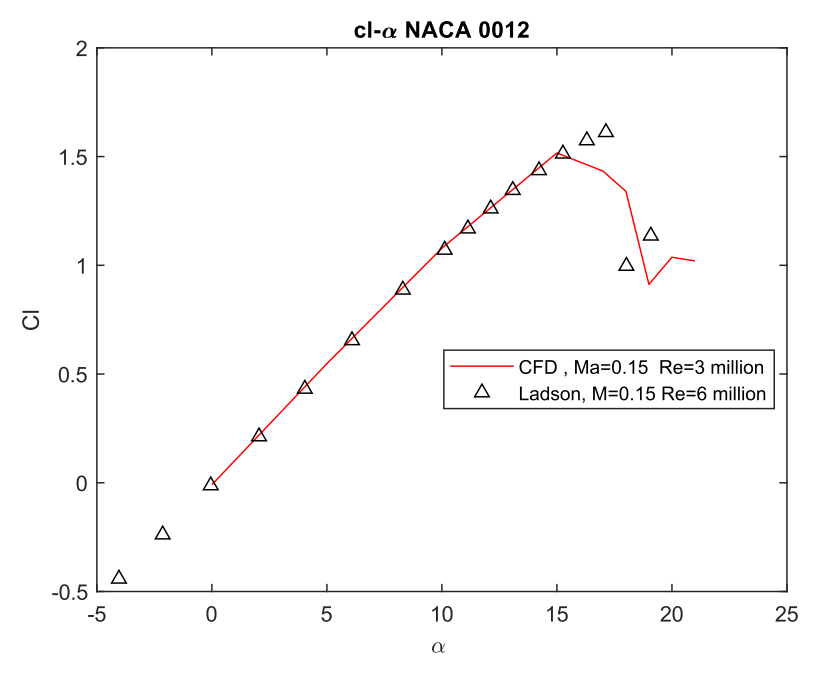


Figure 3.3 - Cl vs α plot, NACA 0012

4. Results

4.1 CFD analysis

In Figure 4.2 it is showed that the actuator becomes effective in the reduction of separation if sufficient momentum is conveyed to the flow: the first row of the picture represents two conditions where separation is present on the rudder. On the upper right, v_{MAX} is 50 m/s but no differences are obtained with respect to AFC-off condition (upper left). At the bottom, on the left, v_{MAX} of 75 m/s is able to reduce separation but not to eliminate it; the flow is completely attached for v_{MAX} of 100 m/s, at the bottom on the right.

In (6), it is defined the increment in sideforce coefficient, ΔC_y , as a measure of the lift enhancement that the actuator provides to the tail section.

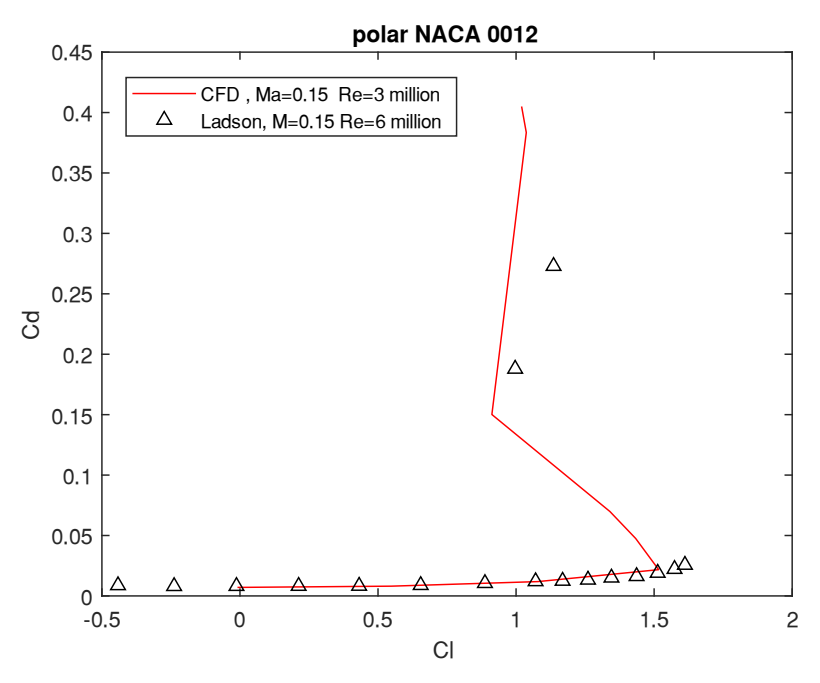


Figure 4.1 - Cd vs Cl plot, NACA 0012

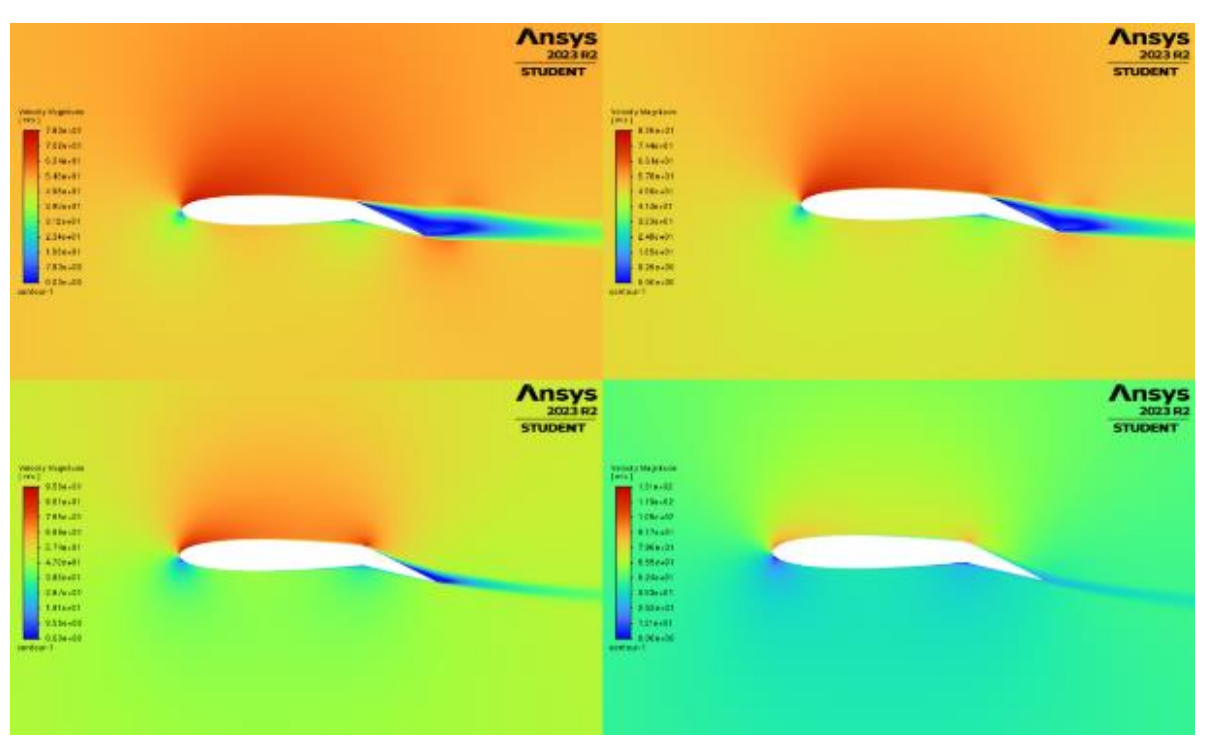


Figure 4.2 - velocity magnitude contours, β =0°, δ =20°, f=100 Hz; left to right, top to bottom, v_{MAX} is 0, 50, 75, 100 m/s respectively

$$\Delta C_{y} = \frac{(C_{y}^{AFC-OR} - C_{y}^{AFC-Off})}{|C_{y}^{AFC-Off}|} \tag{6}$$

Where C_y^{AFC-On} is the lift coefficient when the AFC is active, and $C_y^{AFC-Off}$ when it is switched off. In Figure 4.3, the sideforce enhancement ΔC_y is represented as a function of the output maximum velocity v_{MAX} of the actuator, for a rudder deflection δ of 20° and f=100 Hz: in blue the results when β is 0°, in red when it is 10°. For a fixed deflection angle of 20°, the bigger the sideslip angle, the more important the separation, the more is the effort (v_{MAX}) needed to improve effectiveness of the

surface. Considerable increment in the lifting force is reached as v_{MAX} increases: when $v_{MAX} = 100 \, m/s$, $\Delta C_v = +100 \, \%$ for the blue line, $\Delta C_v = +30\%$ for the red line, Figure 4.3.

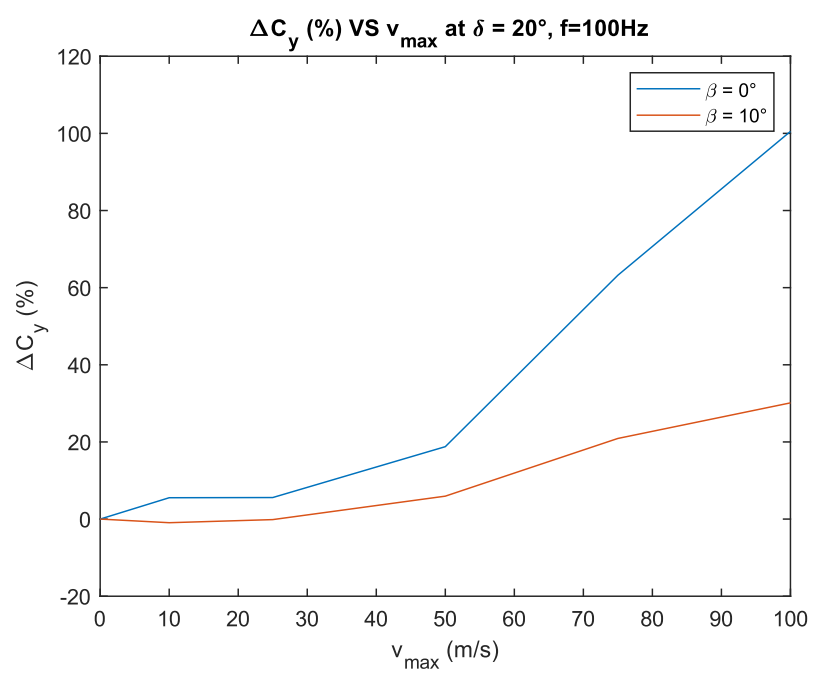


Figure 4.3 - side force enhancement as a function of v_{MAX} , $\delta = 20^{\circ}$

The energy consumption of the active flow control (AFC) system is dependent not only on the velocity of ejection v_{MAX} , but also on the percentage of time over a period of sweeping %t which the AFC is turned on. As an example, here it is considered a flight condition at Mach number (M) 0.15 and Reynolds' number (Re) 15 million, angle of sideslip β of 10°, deflection angle of the rudder δ of 20°. The frequency of sweeping f, i.e. a measure of the period of sweeping of the SJ device, is 100 Hz. The values of maximum velocity of ejection v_{MAX} are 50 m/s, 75 m/s, 100 m/s.

The percentage of time of ejection across the time period of sweeping is defined as follows:

$$\%t = \frac{t_{on}}{T}\% \tag{7}$$

Where t_{on} is the time that the AFC is on, and T is the period of oscillation of the jet.

Figure 4.4 shows the velocity of ejection as a function of time in seconds for %t = 25% and %t = 75%, on the left and on the right respectively.

The power of a jet is proportional to the cube of the velocity; and for this 2D case of study it can be referred to a unit length in meters and calculated as follows:

$$P = \frac{1}{2}\rho v^3 l_{STEP} \tag{8}$$

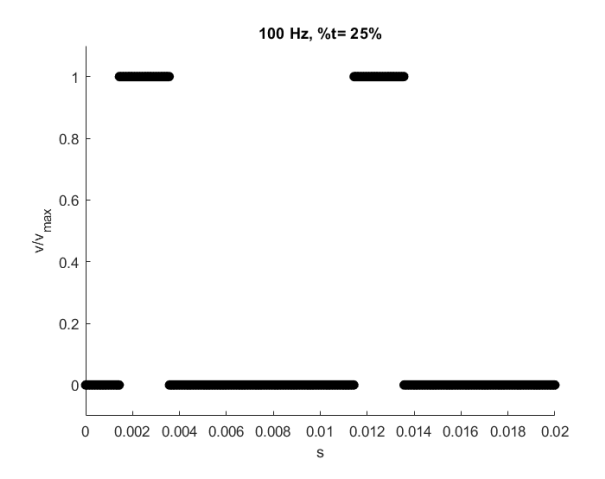
Where ρ is the density and v is the velocity of ejection at the nozzle, and l_{STEP} is the height of the step. The power per unit length is measured in [W/m].

The power coefficient can be defined as:

$$C_{\pi} = \frac{2P}{\rho_{\infty} v_{\infty}^3 c_{MAC}} \tag{9}$$

Where v_{∞} is the farfield velocity, ρ_{∞} the farfield density and c_{MAC} is the mean aerodynamic chord of the airfoil.

The energy is the integral of the instantaneous power in time. For this specific case v_{MAX} is fixed and the power is either constant, if the system is on, or null, when the device is off.



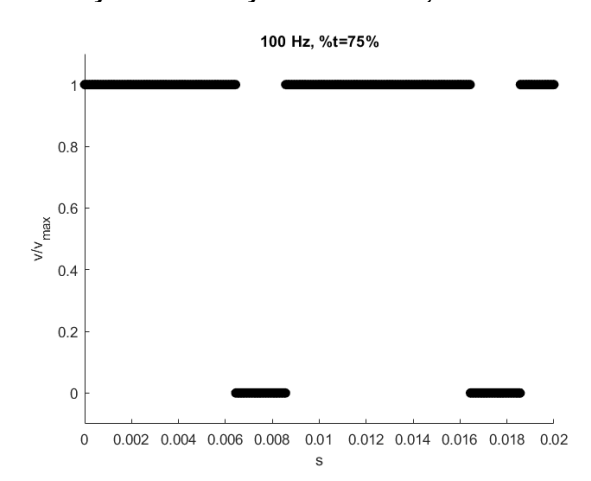


Figure 4.4 - the velocity of ejection as a function of time (seconds) for %t=25% (left), and %t=75% (right)

Therefore, the energy E per unit length ([J/m]) consumed during the sweeping cycle is the product between the power and the total time the device is active during one cycle:

$$E = P * t_{on} \tag{10}$$

By considering the way that t_{on} and P are non dimensionalized in (7) and (9) respectively, then the non-dimensional energy coefficient C_E can be obtained from (10) as follows:

$$C_E = \%t * C_{\pi} \tag{11}$$

In Figure 4.5, it is displayed the behaviour of \mathcal{C}_y with respect to the energy coefficient \mathcal{C}_E , for v_{MAX} of 50, 75 and 100 m/s and for %t from 0% to 100%. It is observed the effect of %t: the blue line (50 m/s) does not cross any different line, the red line (75 m/s) intersects the black line (100 m/s) when \mathcal{C}_E is about 0.005. Over this value, with the same energy consuming the velocity of ejection of 75 m/s at high %t, produces higher \mathcal{C}_y then v_{MAX} of 100 m/s at low %t.

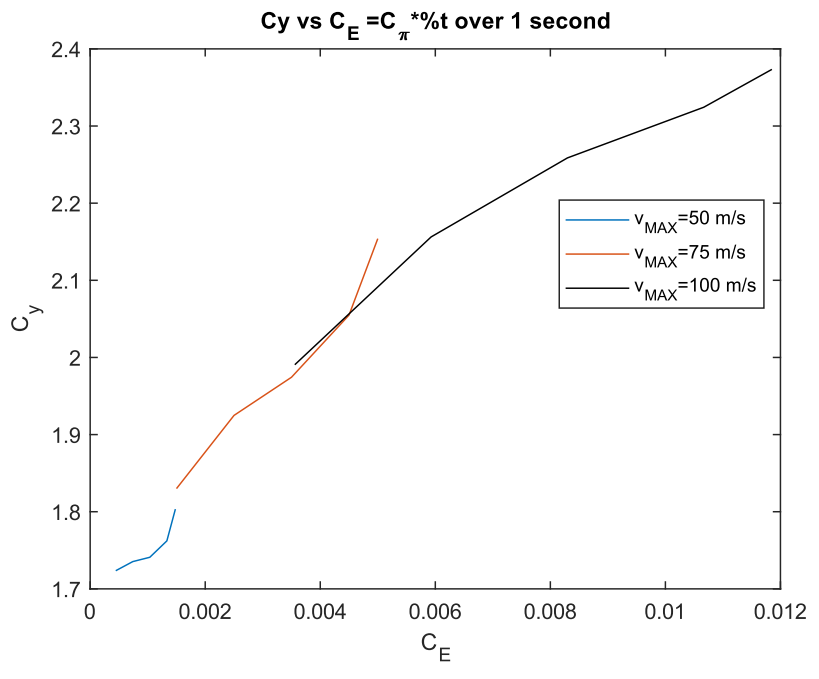


Figure 4.5 - C_v vs C_E

This result leads to the conclusion that it is possible to obtain the same lift coefficient for different values of v_{MAX} when %t is changed. For a fixed flight condition, the best AFC-on solution among the others is the most efficient in terms of energy coefficient.

4.2 Neural Network quality

The network was trained and its quality in predicting the aerodynamic coefficients is demonstrated by the plots in Figure 4.6 and Figure 4.7.

In Figure 4.6, the behaviour of the MSE, (5), versus the iterations (epochs) of the training algorithm is plotted in logarithmic scale: the training set, the validation set, and the testing set are in blue, green and red respectively. At epoch 36, it is obtained the lowest MSE on the validation set: the group of weights and biases of this specific iteration are chosen as final values for the network. The value of the MSE is of the order of e-04, and this means that the CFD target output values are captured quite well by the network outputs.

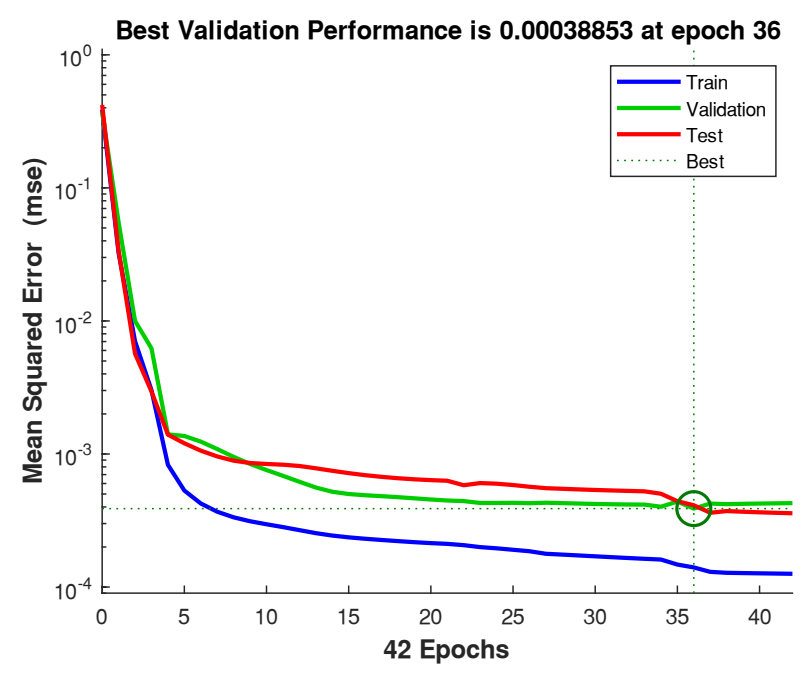


Figure 4.6 - MSE behaviour in log scale during the training

In Figure 4.7, regression lines are represented between the network outputs and the target aerodynamic coefficients from CFD: the training set, the validation set, and the testing set colours are coherent with Figure 4.6. In black, all the up-mentioned data are collected in a single plot. Regression slopes are 1 and offsets are almost null, in every plot: the network can predict well the aerodynamic coefficients.

Consistently with the boundary values of the CFD database, the possible ranges of inputs that can be simulated are (as described in section 3):

- Flap deflections δ from 0° to 20°
- Sideslip angles β from 0° to 10°
- Maximum exit SJ velocities from 0 m/s to 100 m/s
- SJ Frequences between 50 Hz and 150 Hz

4.3 Neural Network applications

The NN was first applied to obtain a sideforce enhancement, ΔC_y , of +20%, in a flight condition of Re 15 million and M 0.15, for sideslip angles from 0° to 10°, and for deflection angles from 10° to 20°. This value of ΔC_y has been chosen as an example for studying the entire process. Other targets can be obviously taken according to a deeply flight mechanics investigation of the manoeuver. The frequency of sweeping was fixed at 100 Hz and a 3D surface of v_{MAX} was obtained as a function of δ

and β , Figure 4.8. The yellow peak shows a region where the highest effort is needed to obtain the +20% enhancement because the flow is not separated for that combination of the two x-y coordinated of the plot. On the other hand, the dark blue valley represents combinations of angles (β , δ) where the v_{MAX} demand is the lowest. For deflections angles between 18° and 20°, the dark blue becomes lighter as β is more and more high: separation is growing, and more power is needed to keep the flow attached.

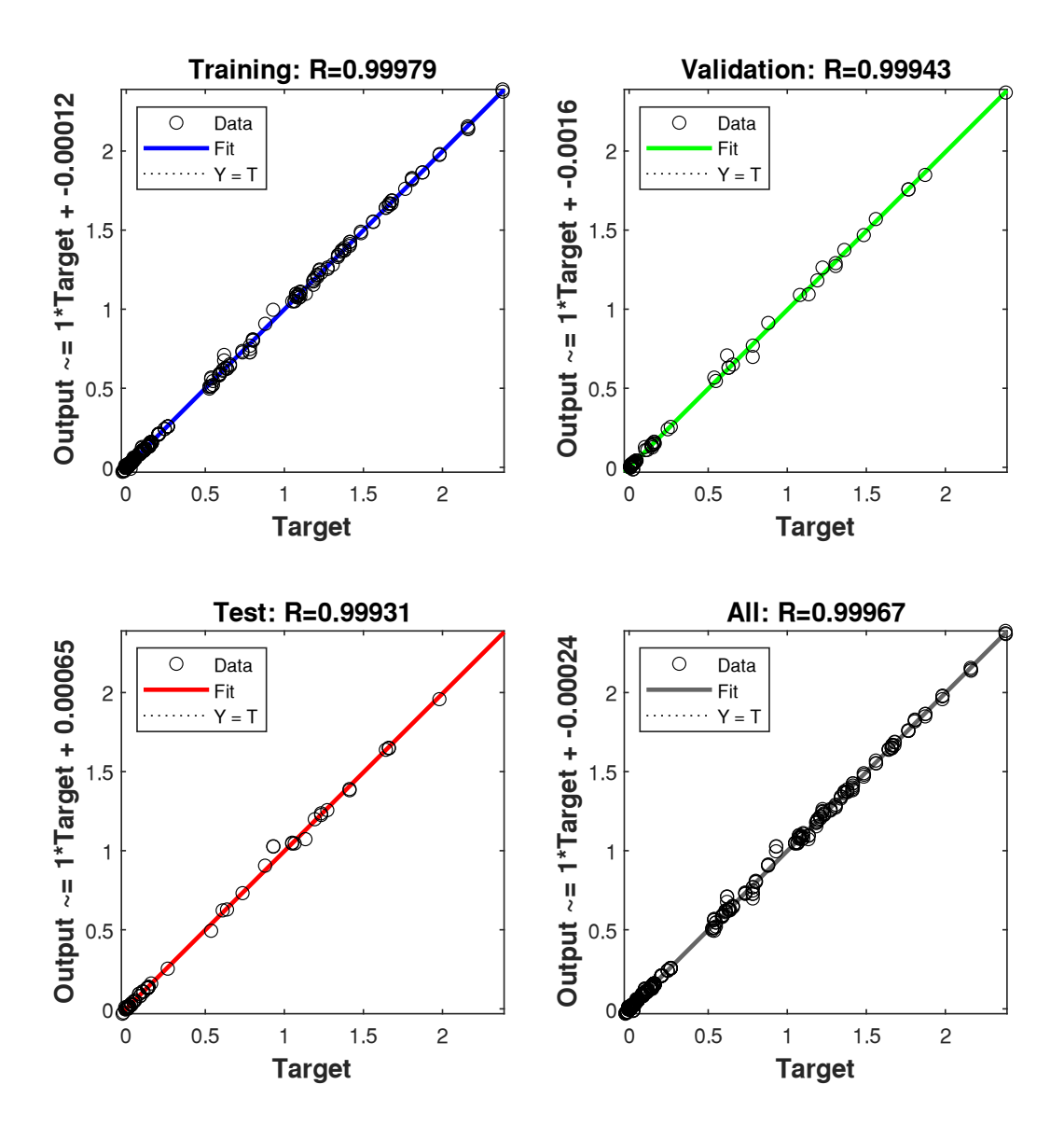


Figure 4.7 - regression plots of the values predicted by the network against the CFD target values

In Figure 4.9, the data from the 3D surface are represented on 2D plots: the ejection speed is showed as a function of δ , and the fixed parameter is the sideslip angle β . For rudder deflections from 10° to 16°, separation is not present when sideslip angle is low: at β =0°, v_{MAX} = 100 m/s is needed to provide 20% side force increment. For sideslip angles from 2° to 4°, a progressive reduction in the needed speed is visible when δ is between 10° and 18°. Over β = 6°, separation on the rudder becomes important even when δ is 10° and it grows as the rudder angle does: v_{MAX} shows a rise with δ as well. Overall, for sideslip angles up to 4°, the effort to increment the lift becomes smaller as the rudder angle δ increases; on the other hand, for β higher than 6°, the effort (v_{MAX}) increases with δ : violet curve, β =6°, and green curve, β =10°, in Figure 4.9, clearly show a monotonically increase in supplied flow to counter act separation.

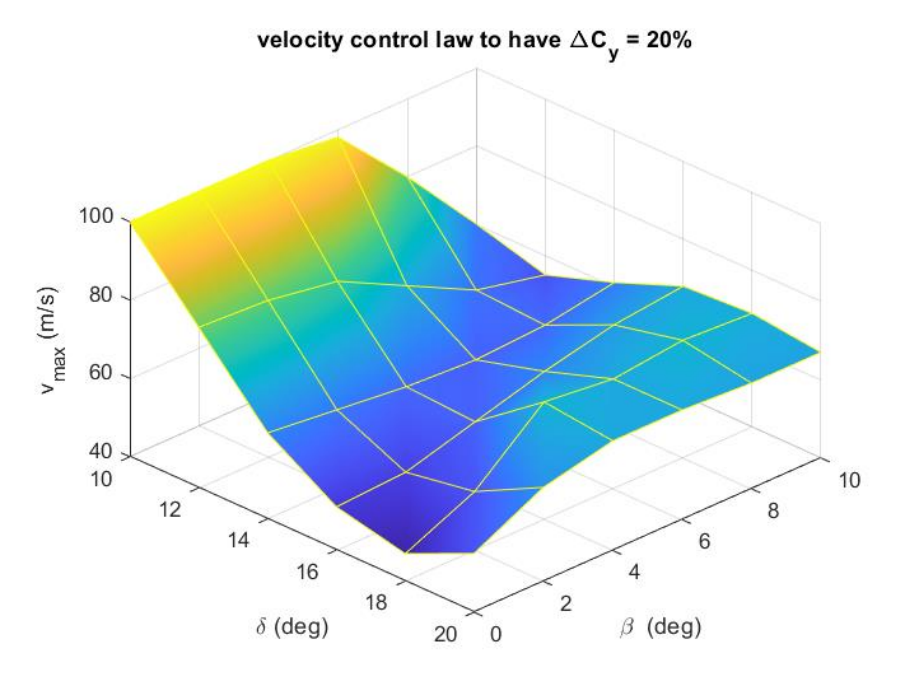


Figure 4.8 - v_{MAX} 3D surface to obtain $\Delta C_v = 20\%$

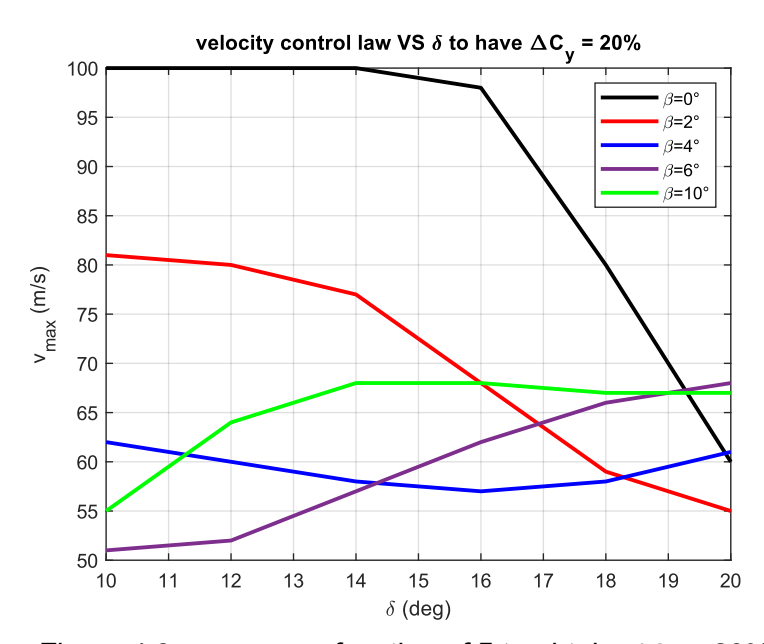


Figure 4.9 - v_{MAX} as a function of δ to obtain $\Delta C_v = 20\%$

As a second example, the neural network was employed to obtain a target lift coefficient Cl of 1.5, Figure 4.10. The value of Cl=1.5 has been chosen as an example for studying the entire process. Other targets can be obviously taken according to a deeply flight mechanics investigation of the manoeuver. The variable parameters are the sideslip angle, the rudder deflection and the ejection velocity. The frequency is kept fixed at 100 Hz. The ejection velocities are 50 m/s, in green, 70 m/s in red, and 100 m/s, in black. Among the others, the lowest isolated-airfoil drag solution corresponds to null sideslip, rudder deflection of 20°, and velocity of 100 m/s: the airfoil NN drag coefficient is 0.36e-2.

Moreover, flying with no sideslip is optimal for the overall drag of the airplane: in Table 3, the CFD airfoil drag coefficients are listed, for different flight conditions producing Cl=1.5. In the first two rows of Table 3, the AFC device is off: when δ =0°, the β =0° drag is obtained from the polar of Figure 4.1. The last row of the table is the above AFC-on condition, which produces an airfoil CFD Cd = 0.830e-2: this value is considerably lower than the other two. Therefore, the AFC-on null sideslip and δ =20° combination guarantees to recover the target performance (Cl = 1.5), without any airplane yaw angle, so minimizing the overall drag.

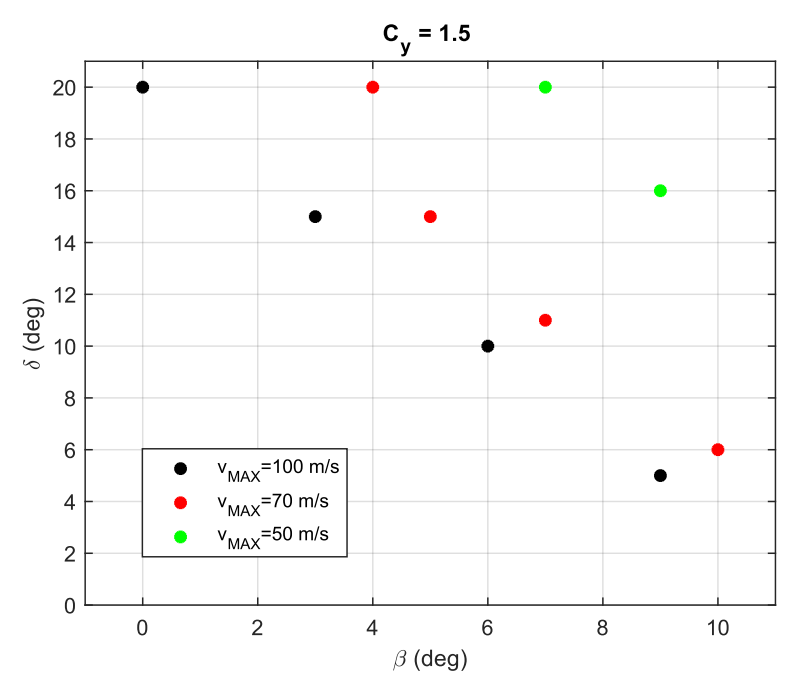


Figure 4.10 - δ and β combination to obtain $C_v = 1.5$, for variable v_{MAX} and fixed f=100 Hz

Table 3 [Cl=1.5, M=0.15, Re=15 mil]						
β	δ	v_{MAX}	Cd			
15°	0°	0 m/s	2.335e-2			
8°	20°	0 m/s	5.116e-2			
0°	20°	100 m/s	0.830e-02			

In both the NN applications, results were retrieved in a time of the order of 1 second, each flow configuration: Al allowed to save time, with respect to performing CFD simulations for all the combinations of parameters.

5. Conclusions and follow-on

A new methodology of applying machine learning to a simplified model of an active flow control (AFC) system on a 2D flapped airfoil was explored.

CFD results, obtained by solving 2D U-RANS and k-ω SST equations with ANSYS FLUENT ©. demonstrated that this AFC technology produces significant sideforce increments when separation is reduced on the rudder section.

CFD results were collected in a dataset, and they were employed successfully in MATLAB © for the training of a Neural Network (NN) of 4 inputs, 10 neurons and 3 outputs. The MSE, between the NN outputs and the target CFD outputs, was of the order of e-04, and regression plots proved that the network can accurately predict the aerodynamic coefficients as required for covering the entire flight envelope, in a well-defined range of the input parameters, and within the boundaries previously defined by standard CFD methods.

The NN was applied, at Re 15 million and M 0.15, firstly to obtain SJ parametres suitable to guarantee a target sideforce increment of +20%, and secondly, it was exploited to find the most suitable set of SJ function parameters able to reach a target Cl=1.5.

This work proved the immediate advantage that a Neural Network, if properly trained, allows to estimate aerodynamic coefficients with a very less computational effort and in a considerably smaller amount of time with respect to a pure-CFD approach.

The natural development of this research is to extend the present analysis at the 3D environment, with the final aim to set not only the exit flow parameters of each SJ device but, above all, to identify the spanwise number and their relative position to maximize efficiency of the entire vertical surface.

6. Contact Author Email Address

Mail to: carlo2.cordoni@mail.polimi.it

7. Copyright Statement

The authors confirm that they, and/or their company or organization, hold copyright on all of the original material included in this paper. The authors also confirm that they have obtained permission, from the copyright holder of any third party material included in this paper, to publish it as part of their paper. The authors confirm that they give permission, or have obtained permission from the copyright holder of this paper, for the publication and distribution of this paper as part of the ICAS proceedings or as individual off-prints from the proceedings.

References

- [1] Stouffer, R. (1979). Oscillating spray device. U.S. Patent 4151955.
- [2] Jones, G. S., Milholen, W. E., & al. (2017). A Sweeping jet application on a high Reynolds' number Semispan supercritical wing configuration. *35th AIAA applied aerodynamics conference, Denver, Colorado, 5-9 June, 2017.*
- [3] Whalen, E., Lacy, D., Lin, J., Andino, M., Washbu, A., Graff, E., & Wygnanski, I. (2015). Performance enhancement of a full-scale vertical tail model equipped with Active Flow Control. *AIAA 2015-0784,53rd AIAA Aerospace Sciences Meeting, Kissimmee, Florida, 5-9 January 2015*
- [4] Whalen, E. A., Shmilovich, A., Spoor, M., Tran, J., Vijgen, P., Lin, J. C., & Andino, M. (2016). Flight test of an AFC enhanced vertical tail. *AIAA Journal Volume 56, Number 9, September 2018*, pp. 3393–3398
- [5] Hagan, M. T., & Menhaj, M. B. (1994). Training feedforward networks with the Marquardt algorithm. *IEEE Transactions on Neural Networks*.
- [6] Ladson, C. L., Hill, A. S., & Johnson, W. G. (1987). Pressure distributions from high Reynolds number transonic tests of an NACA 0012 airfoil in the Langley 0.3-meter transonic cryogenic tunnel. *NASA Technical Memorandum* (*TM*) 100526.
- [7] McCroskey. (1987). A critical assessment of a wind tunnel results for the NACA 0012 airfoil. *NASA Technical Memorandum 10001*.
- [8] Jeong, H. S., & Kim, K. Y. (2018). Shape optimization of a feedback-channel fluidic oscillator. *Engineering Applications of Computational Fluid Mechanics*, 12:1, 169-181.
- [9] Koklu, M. (2018). Effects of Sweeping Jet Actuator Parameters on Flow Separation Control. *AIAA Journal*, <u>Volume</u> 56, <u>Number 1</u>, <u>January 2018</u>, pp.100-110
- [10] Melton, L. P., & Koklu, M. (2016). Active Flow Control using Sweeping Jet Actuators on a Semi-span Wing Model. 54th AIAA aerospace science meeting, San Diego, January 4-8, 2016.
- [11] Seele, R., Graff, E., Lin, J., & Wygnanski, I. (2013). Performance Enhancement of a Vertical Tail Model with Sweeping Jet Actuators. 51st AIAA Aerospace Sciences Meeting including the New Horizons Forum and Aerospace Exposition, Grapevine (Dallas/Ft. Worth Region), Texas, January 7-10, 2013
- [12] Joshi, S. N., & Gujarathi, Y. S. (2016). A Review on Active and Passive Flow Control Techniques. *International Journal on Recent Technologies in Mechanical and Electrical Engineering*, 3(4), 01–06.
- [13] Kim, S. H., & Kim, K. Y. (2019). Effects of Installation Conditions of Fluidic Oscillators on Control of Flow Separation. *AIAA Journal Volume 57*, *Number 12,December 2019*, pp. 5208–5219.
- [14] Kim, S.-H., & Kim, K.-Y. (2020). Effects of installation location of fluidic oscillators on aerodynamic performance of an airfoil. *Aerospace Science and Technology Volume 99, April 2020*.
- [15] Koklu, M., & Owens, L. R. (2014). Flow separation control over a ramp using weeping jet actuators. 7th AIAA flow control conference, Atlanta Georgia, June 16-20, 2014.
- [16] Melton, P. L., Koklu, M., Andino, M., Lin, J. C., & Edelman, L. (2016). Sweeping Jet Optimization Studies. 8th AIAA Flow Control Conference, Washington D.C.13-17 June, 2016.
- [17] Menter, F. R. (1994). Two-Equation Eddy-Viscosity Turbulence Models for Engineering Applications. *AIAA Journal,Volume 32,Number 8,August 1984, pp. 1598–1605*
- [18] Seele, R., Graff, E., Gharib, M., Taubert, L., Lin, J., & Wygnanski, I. (2012). Improving Rudder Effectiveness with Sweeping Jet Actuators. 6th AIAA Flow Control Conference, New Orleans, Louisiana, 25-28 June 2012.
- [19] Shmilovich, A., & Vatsa, V. N. (2019). Practical Computational Methods for Airplanes with Flow-Control

A CFD study of an AFC system on a VTS, with the aid of Al.

- Systems. AIAA Journal, Volume 57, Number 1, January 2019, pp. 35–52
- [20] Shmilovich, A., Yadlin, Y., & Whalen, E. A. (2016). Numerical Simulations of an Airplane with an Active Flow Control System. 8th AIAA Flow Control Conference, Washington D.C.13-17 June, 2016.
- [21] Woszidlo, R., & Wygnanski, I. (2011). Parameters Governing Separation Control with Sweeping Jet Actuators. 29th AIAA Applied Aerodynamics Conference, Honolulu, Hawaii, June 27-30, 2011.
- [22] Cordoni C. (2024), A machine learning methodology to predict the aerodynamic performances of an Active Flow Control system on a 2D airfoil. Master thesis at Politecnico di Milano.